ISSN 1674-1056
http://cpb.iphy.ac.cn
http://iopscience.iop.org/cpb
中国物理 B
Chinese Physics
中国物理
Chinese Physics B

Effect of Mn doping on mechanical properties and electronic structure of WCoB ternary boride by first-principle calculations

Tong Zhang(张桐), Hai-Qing Yin(尹海清), Cong Zhang(张聪), Xuan-Hui Qu(曲选辉), Qing-Jun Zheng(郑清军)
Citation: Chin. Phys. B . 2018, 27(10): 107101. **doi:** 10.1088/1674-1056/27/10/107101

Journal homepage: http://cpb.iphy.ac.cn; http://iopscience.iop.org/cpb

What follows is a list of articles you may be interested in

First principles study of stability, mechanical and electronic properties of chromium silicides

Bo Ren(任博), De-Hong Lu(卢德宏), Rong Zhou(周荣), De-Peng Ji(姬德朋), Ming-Yu Hu(胡明钰), Jing Feng(冯晶)
Chin. Phys. B . 2018, 27(10): 107102. **doi:** 10.1088/1674-1056/27/10/107102

Anisotropic elastic properties and ideal uniaxial compressive strength of TiB_2 from first principles calculations

Min Sun(孙敏), Chong-Yu Wang(王崇愚), Ji-Ping Liu(刘吉平)
Chin. Phys. B . 2018, 27(7): 077103. **doi:** 10.1088/1674-1056/27/7/077103

Electronic structures and optical properties of HfO_2-TiO_2 alloys studied by first-principles GGA+ *U* approach

Jin-Ping Li(李金平), Song-He Meng(孟松鹤), Cheng Yang(杨程), Han-Tao Lu(陆汉涛), Takami Tohyama(遠山貴巳)
Chin. Phys. B . 2018, 27(2): 027101. **doi:** 10.1088/1674-1056/27/2/027101

Optical properties of anatase and rutile TiO_2 studied by GGA+*U*

Jinping Li(李金平), Songhe Meng(孟松鹤), Liyuan Qin(秦丽媛), Hantao Lu(陆汉涛)
Chin. Phys. B . 2017, 26(8): 087101. **doi:** 10.1088/1674-1056/26/8/087101

Visible light absorption of (Fe, C/N) co-doped $NaTaO_3$: DFT+*U*

Peng-Li Tian(田鹏莉), Zhen-Yi Jiang(姜振益), Xiao-Dong Zhang(张小东), Bo Zhou(周波), Ya-Ru Dong(董亚茹), Rui Liu(刘睿)
Chin. Phys. B . 2017, 26(8): 087102. **doi:** 10.1088/1674-1056/26/8/087102

Effect of Mn doping on mechanical properties and electronic structure of WCoB ternary boride by first-principles calculations*

Tong Zhang(张桐)[1,2], Hai-Qing Yin(尹海清)[1,2,†], Cong Zhang(张聪)[1], Xuan-Hui Qu(曲选辉)[1,2], and Qing-Jun Zheng(郑清军)[3]

[1] *Collaborative Innovation Center of Steel Technology, University of Science and Technology Beijing, Beijing* 100083, *China*,
[2] *Beijing Key Laboratory of Materials Genome Initiative, University of Science and Technology Beijing, Beijing* 100083, *China*,
[3] *Kennametal Inc*, 1600 *Technology Way, PA* 15650, *USA*

(Received 17 April 2018; revised manuscript received 20 July 2018; published online 10 September 2018)

The first-principles calculations are performed to investigate the structural, mechanical property, hardness, and electronic structure of WCoB with 0, 8.33, 16.67, 25, and 33.33 at.% Mn doping content and W_2CoB_2 with 0, 10, and 20 at.% Mn doping content. The cohesive energy and formation energy indicate that all the structures can retain good structural stability. According to the calculated elastic constants, Mn is responsible for the increase of ductility and Poisson's ratio and the decrease of Young's modulus, shear modulus, and bulk modulus. By using the population analysis and mechanical properties, the hardness is characterized through using the five hardness models and is found to decrease with the Mn doping content increasing. The calculated electronic structure indicates that the formation of a B–Mn covalent bond and a W–Mn metallic bond contribute to the decreasing of the mechanical properties.

Keywords: Mn doping, WCoB, electronic structure, first-principles calculations

PACS: 71.15.Dx, 78.20.Bh **DOI:** 10.1088/1674-1056/27/10/107101

1. Introduction

Transition metal borides have high hardness, high melting point, relatively high electrical conductivity, and corrosion resistance, which have been promising candidates for wear resistance applications.[1–3] Reaction bronizing sintering[4,5] has been developed to solve the poor sintering property of ternary boride and used to fabricate ternary borides WCoB, Mo_2FeB_2, and Mo_2NiB_2,[6] which have received a great deal of attention in recent years.

Among them, WCoB exhibits the high hardness and outstanding mechanical properties, and has been studied for years.[7–9] Microalloying is an important method to improve the mechanical properties and microstructure of alloys. For ternary boride hard alloy, there are some transition elements used to improve its overall mechanical properties, such as Cr, V, Mn, Ni, Nb, etc.[10–15] There is no doubt that Mn is an important alloying element for ternary boride. Yang[16] found that 10 wt% Mn doping can improve the transverse rupture strength (TRS) and hardness of Mo_2FeB_2 hard alloy from 980 MPa, 87.4 HRA to 1290 MPa, 89.4 HRA by solid solution strengthening and grain refinement. Takagi[17] found that 2.5 wt% Mn doping improves the TRS of Mo_2NiB_2 hard alloy to a maximum value of 3500 MPa, and 10 wt% Mn doping contributes to the highest hardness of 88 HRA. Komai[18] found 15 wt% Cr doping improves the TRS and hardness of WCoB hard alloy from 1820 MPa, 78 HRA to the maximum value of 2850 MPa, 89 HRA, respectively. Ke[19] proved that 0.3 wt% VC and 0.3 wt% Cr_3C_2 doping WCoB-TiC hard alloy show the maximum mechanical properties (hardness, TRS, and K_{IC} are 92.6 HRA, 1976 MPa, and 14.8 MPa·$m^{1/2}$, respectively). Although some researchers study the influence of Mn doping on Mo_2FeB_2 or Mo_2NiB_2 ternary boride hard alloys, there has been no study on Mn doping WCoB ternary boride, which could be a useful way to improve mechanical properties of WCoB hard alloy.

The first-principles simulation has been widely used to explore the band structure, molecular structure, and electronic properties in recent years.[20–23] It is an advanced way to explore the effect of the alloying element doping ternary boride. The doping content of the alloying element plays an important role in the experimental research. So it is meaningful to find a suitable doping content value in Mn doping WCoB ternary boride hard alloy by using a theoretical method. Lin[24] found alloying elements Mn, Ni, and Cr prefer to occupy the Fe site of Mo_2FeB_2 and Ni improves its ductility while Cr increases the hardness and Young's modulus. However, only 10 at.%. Mn, Ni, and Cr doping content is not enough to explore the influence of alloying element doping. Therefore, Wang[25] chose

*Project supported by the National Key Research and Development Program, China (Grant No. 2016YFB0700503), the National High Technology Research and Development Program of China (Grant No. 2015AA034201), the Beijing Science and Technology Plan, China (Grant No. D161100002416001), the National Natural Science Foundation of China (Grant No. 51172018), and the Kennametal Inc., China.

†Corresponding author. E-mail: hqyin@ustb.edu.cn

© 2018 Chinese Physical Society and IOP Publishing Ltd

2.5, 5, 10, and 20 at.% doping content to explore the influence of Cr and Ni on the Mo_2FeB_2 hard alloy. They found that the Ni can reduce the hardness and improve the ductility by increasing the alloying content, and Cr can increase the Young's modulus and hardness, and it reduces the ductility by increasing the alloying content. Nevertheless, there is no study on Mn doping WCoB ternary boride hard alloy either; such a study can provide a theoretical basis for experimental studies on WCoB.

In this paper, the first-principles method is used to investigate the influence of Mn doping content on the mechanical properties of WCoB ternary boride. Since W_2CoB_2 coexists in WCoB hard alloy, which has been proved by Xu,[26] the effect of Mn on the mechanical properties and also on the electronic structure of W_2CoB_2 are also studied by first principles. We consider the two cases, i.e. the content values of Mn are 0, 8.33, 16.67, 25, and 33.33 at.% separately in WCoB unit-cell, and the content values of Mn are 0, 10, and 20 at.% separately in the W_2CoB_2 unit-cell. The structure, elastic property, hardness, and electronic structure of WCoB and W_2CoB_2 at various doping content values are studied in detail.

2. Methods and models

All simulations in this paper are performed by using density functional theory (DFT),[27] with the help of the Cambridge Serial Total Energy Package (CASTEP) code.[28] The generalized gradient approximation (GGA) and Perdew–Burke–Ernzerh (PBE) scheme are used to evaluate the exchange and correlation function.[29] The interaction between valence electrons and the ionic cores is treated with the Vanderbilt ultrasoft pseudopotential.[30] The electronic configurations are chosen as W ($5s^25p^65d^46s^2$), Co ($3d^74s^2$), B ($2s^22p^1$), and Mn ($3d^54s^2$). The WCoB possesses a space group of Pnma (No. 62, ICSD collection code: 613390)[31] with an orthorhombic structure, and W_2CoB_2 possesses a space group of Immm (No. 71, ICSD collection code: 16776)[32] with an orthorhombic structure. The lattice parameters of WCoB are $a = 5.745$ Å, $b = 3.203$ Å, and $c = 6.652$ Å, and the Wyckoff positions of W, Co, and B are 4*c* (0.021, 0.25, 0.18), 4*c* (0.142, 0.25, 0.561), and 4*c* (0.765, 0.25, 0.623). The lattice parameters of W_2CoB_2 are $a = 7.075$ Å, $b = 4.564$ Å, and $c = 3.177$ Å and the Wyckoff positions of W, Co, and B are 4*f* (0.205, 0.5, 0), 2*a* (0, 0, 0), and 4*h* (0, 0.3, 0.5), respectively.

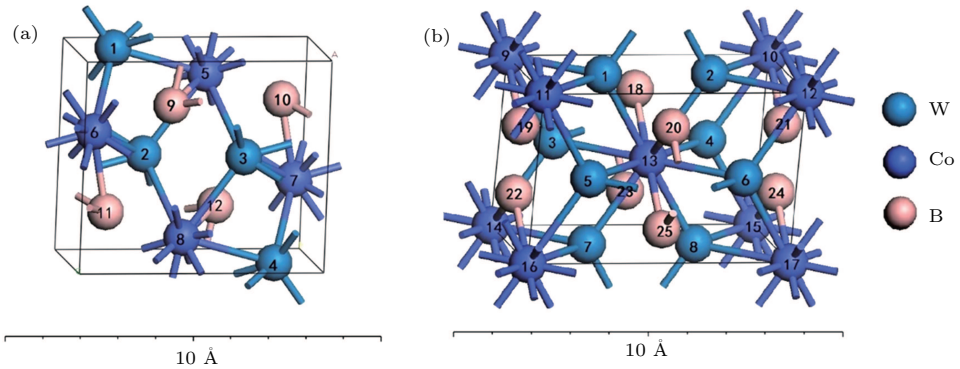


Fig. 1. (color online) Orthorhombic structure of Mn doping (a) WCoB ($W_4Co_{4-x}Mn_xB_4$, $x = 0, 1, 2, 3, 4$) and (b) W_2CoB_2 ($W_4Co_{2-x}Mn_xB_4$, $x = 0, 1, 2$).

To investigate the influence of Mn doping content for WCoB and W_2CoB_2, we choose different numbers of Mn atoms to replace Co site positions, because of the similar atom radius of Mn ($r = 161$ pm) and Co ($r = 152$ pm). By replacing 0, 1, 2, 3, and 4 Co atoms in the WCoB unit-cell, the chemical formulas can be denoted by a-$W_4Co_4B_4$, b-$W_4Co_3MnB_4$ (position: 5), c-$W_4Co_2Mn_2B_4$-symmetry (position: 5, 8), d-$W_4Co_2Mn_2B_4$-unsymmetry (position: 5, 7), e-$W_4CoMn_3B_4$ (position: 5, 6, 7), and f-$_4Mn_4B_4$ (position: 5, 6, 7, 8). By replacing 0, 1, and 2 Co atoms in the W_2CoB_2 unit-cell, the chemical formulas can be denoted by g-$W_4Co_2B_4$, h-W_4CoMnB_4 (position: 13), and i-$W_4Mn_2B_4$ (position: 9, 10, 11, 12, 13, 14, 15, 16, 17), which are shown in Fig. 1. A plane-wave basis set for electron wave function with a cutoff energy of 550 eV is employed, and the *k*-point mesh which is used to integrate in the Brillouin zone is performed as 4×8×4 and 3×5×8 for WCoB and W_2CoB_2, respectively. During the geometry optimization, the Broyden–Flecher–Goldfarb–Shanno (BFGS) geometry optimization task is implemented to obtain a stable structure with minimum total energy[33] and fully relaxed atomic position. The self-consistent convergence of the total energy is 5×10^{-6} V/atom and the maximum force on the atom is below 0.01 eV/Å, maximum stress is below 0.02 GPa, and the maximum displacement between cycles is below 5×10^{-4} Å.

3. Results and discussion

3.1. Structural stability

The stability can be used to explore the influence of Mn doping WCoB and W_2CoB_2, which is evaluated by two energy parameters, i.e. cohesive energy E_{coh} and formation energy E_f. The equation of cohesive energy E_{coh} is expressed as

$$E_{\text{coh}} = (E_{\text{total}} - aE_w - bE_{\text{Co}} - cE_{\text{B}} - dE_{\text{Mn}})/(a+b+c+d), \quad (1)$$

where E_{coh} is the cohesive energy of WCoB or W_2CoB_2 per formula, E_{total} is the total energy of Mn doping WCoB and W_2CoB_2 structure, and E_{W}, E_{Co}, E_{B}, and E_{Mn} are the energies of free W, Co, B, and Mn atoms, respectively. The equation of formation energy E_{f} is expressed as

$$E_{\text{f}} = E_{\text{coh}}(\text{cell}) - aE_{\text{coh}}(\text{W}) - bE_{\text{coh}}(\text{Co}) - cE_{\text{coh}}(\text{B}) - dE_{\text{coh}}(\text{Mn}). \quad (2)$$

The cohesive energies of E_{coh}(W), E_{coh}(Co), E_{coh}(B), and E_{coh}(Mn) are selected respectively from elementary substances W (IM3M), Co (P64MMC), B (P4N2), and Mn (P4132), which have the lowest energy. The a, b, c, and d are the numbers of atoms in the WCoB or W_2CoB_2 lattice, respectively.

The cohesive energy is used to evaluate the energy change of a free atom transforming into a compound, so the cohesive energy can indicate the crystal structure stability. The formation enthalpy presents the energy change in the process of simple substances transforming into compounds. Therefore, equations (1) and (2) require negative values of E_{coh} and E_{f}, which indicates the thermodynamically stable structure.

The calculated values of lattice parameters, unit cell volume, cohesive energy, and formation energy for WCoB and W_2CoB_2 are shown in Table 1, together with the available experimental data for comparison. These calculation results show that the calculated structure parameters are consistent with the experimental values, indicating the reliability of the present calculations.

Table 1. Calculated values of lattice parameters, cohesive energy E_{coh} (eV/atom), and formation energy E_{f} (eV/atom) of $W_4Co_{4-x}Mn_xB_4$ and $W_4Co_{2-x}Mn_xB_4$.

WCoB/W_2CoB_2	Lattice constants/Å	V/Å^3	E_{coh}	E_{f}
$W_4Co_4B_4$-ex	$a = 5.746$, $b = 3.203$, $c = 6.652$	122.43	–	–
a-$W_4Co_4B_4$	$a = 5.746$, $b = 3.256$, $c = 6.624$	123.938	–9.363	–0.491
b-$W_4Co_3MnB_4$	$a = 5.752$, $b = 3.254$, $c = 6.703$	125.462	–9.418	–0.467
c-$W_4Co_2Mn_2B_4$	$a = 5.805$, $b = 3.210$, $c = 6.796$	126.614	–9.484	–0.463
d-$W_4Co_2Mn_2B_4$	$a = 3.221$, $b = 5.820$, $c = 6.765$	126.810	–9.476	–0.455
e-$W_4CoMn_3B_4$	$a = 5.857$, $b = 3.188$, $c = 6.864$	128.165	–9.541	–0.451
f-$W_4Mn_4B_4$	$a = 5.878$, $b = 3.170$, $c = 6.956$	129.638	–9.627	–0.454
$W_4Co_2B_4$-ex	$a = 7.075$, $b = 4.564$, $c = 3.177$	102.59	–	–
g-$W_4Co_2B_4$	$a = 7.109$, $b = 4.566$, $c = 3.190$	103.559	–9.503	–0.527
h-W_4CoMnB_4	$a = 7.177$, $b = 4.619$, $c = 3.153$	104.540	–9.568	–0.506
i-$W_4Mn_2B_4$	$a = 7.226$, $b = 4.679$, $c = 3.126$	105.705	–9.653	–0.495

It is obvious that higher Mn doping content leads to the increasing of unit cell volumes, which is caused by the larger atom radius of Mn ($r = 161$ pm) than Co ($r = 152$ pm). The volume change of b-$W_4Co_3MnB_4$, c-$W_4Co_2Mn_2B_4$, d-$W_4Co_2Mn_2B_4$, e-$W_4CoMn_3B_4$, and f-$W_4Mn_4B_4$ are 1.230%, 2.159%, 2.317%, 3.411%, and 4.599%, respectively. Similarly, the volume change of h-W_4CoMnB_4 and i-$W_4Mn_2B_4$ are 0.947% and 2.072%, respectively. A similar trend can be found in the lattice parameters.

The calculated values of cohesive energy of Mn doping WCoB and W_2CoB_2 are negative, indicating all of these compounds are stable. With the increasing of Mn content, the decreasing of cohesive energy means that the Mn doping contributes to the more stable structure of WCoB and W_2CoB_2. It is clear that all the values of the formation energy are negative, implying that all Mn doping compounds are also stable. Moreover, the formation energy increases with the increasing of Mn content, implying the decreasing of the possibility in the formation process from simple substances. This result can be attributed to the Mn doping damage to the integrity of the crystal structure. When all Mn atoms replace Co atoms in the unit cell, the E_{f} increases slightly instead of further increasing. This phenomenon should be derived from the formation of the new stable structures, WMnB and W_2MnB_2. Overall, it can be concluded that all compounds are stable and retain good structural stability at the highest doping content.

3.2. Mechanical properties

In order to study the influence of Mn doping content on WCoB and W_2CoB_2, the elastic constant, Young's modulus, bulk modulus, shear modulus, Poisson's ratio, anisotropic index, and B/G ration are discussed and analyzed, as shown in Tables 2 and 3. The mechanical stability of Mn doping WCoB and W_2CoB_2 should be examined by traditional mechanical stability conditions.[34] WCoB and W_2CoB_2 are orthorhombic crystals, which have nine independent elastic stiffness constants, so the sequence is shown as follows:

$$\begin{aligned} &C_{ii} > 0, \\ &[C_{11} + C_{22} + C_{33} + 2(C_{12} + C_{13} + C_{23})] > 0, \\ &(C_{11} + C_{22} - 2C_{12}) > 0, \\ &(C_{11} + C_{33} - 2C_{13}) > 0, \\ &(C_{22} + C_{33} - 2C_{23}) > 0, \end{aligned} \quad (3)$$

where C_{ij} is the single crystal elastic constant, and S_{ij} is the elastic compliant coefficient, which could be converted from

the corresponding C_{ij} matrix equation.

For orthorhombic phase,[35] B_V, B_R, G_V, and G_R can be expressed by using the following equations:

$$B_R = 1/[(S_{11}+S_{22}+S_{33})+2(S_{12}+S_{13}+S_{23})], \quad (4)$$

$$B_V = (C_{11}+C_{22}+C_{33})/9+2(C_{12}+C_{13}+C_{23})/9, \quad (5)$$

$$G_R = 15/[4(S_{11}+S_{22}+S_{33})-4(S_{12}+S_{13}+S_{23}) +3(S_{44}+S_{55}+S_{66})], \quad (6)$$

$$B_V = (C_{11}+C_{22}+C_{33})/15-(C_{12}-C_{13}-C_{23})/15 +(C_{44}+C_{55}+C_{66})/5. \quad (7)$$

Table 2. Calculated elastic constants (in GPa) of $W_4Co_{4-x}Cr_xB_4$.

	a-$W_4Co_4B_4$	b-$W_4Co_3MnB_4$	c-$W_4Co_2Mn_2B_4$	d-$W_4Co_2Mn_2B_4$	e-$W_4CoMn_3B_4$	f-$W_4Mn_4B_4$
C_{11}	553.47	539.43	535.02	517.78	512.57	516.25
C_{22}	507.66	480.10	476.62	462.16	447.64	444.87
C_{33}	613.82	576.78	570.12	543.94	549.34	536.25
C_{44}	234.88	230.02	229.91	222.44	225.16	225.86
C_{55}	190.13	188.14	182.68	181.58	172.15	165.98
C_{66}	237.06	231.89	240.66	231.89	232.99	242.59
C_{12}	254.82	253.86	261.67	269.53	259.28	255.60
C_{13}	179.12	171.96	159.89	154.41	155.69	148.63
C_{23}	217.25	209.08	218.16	217.31	200.90	191.86

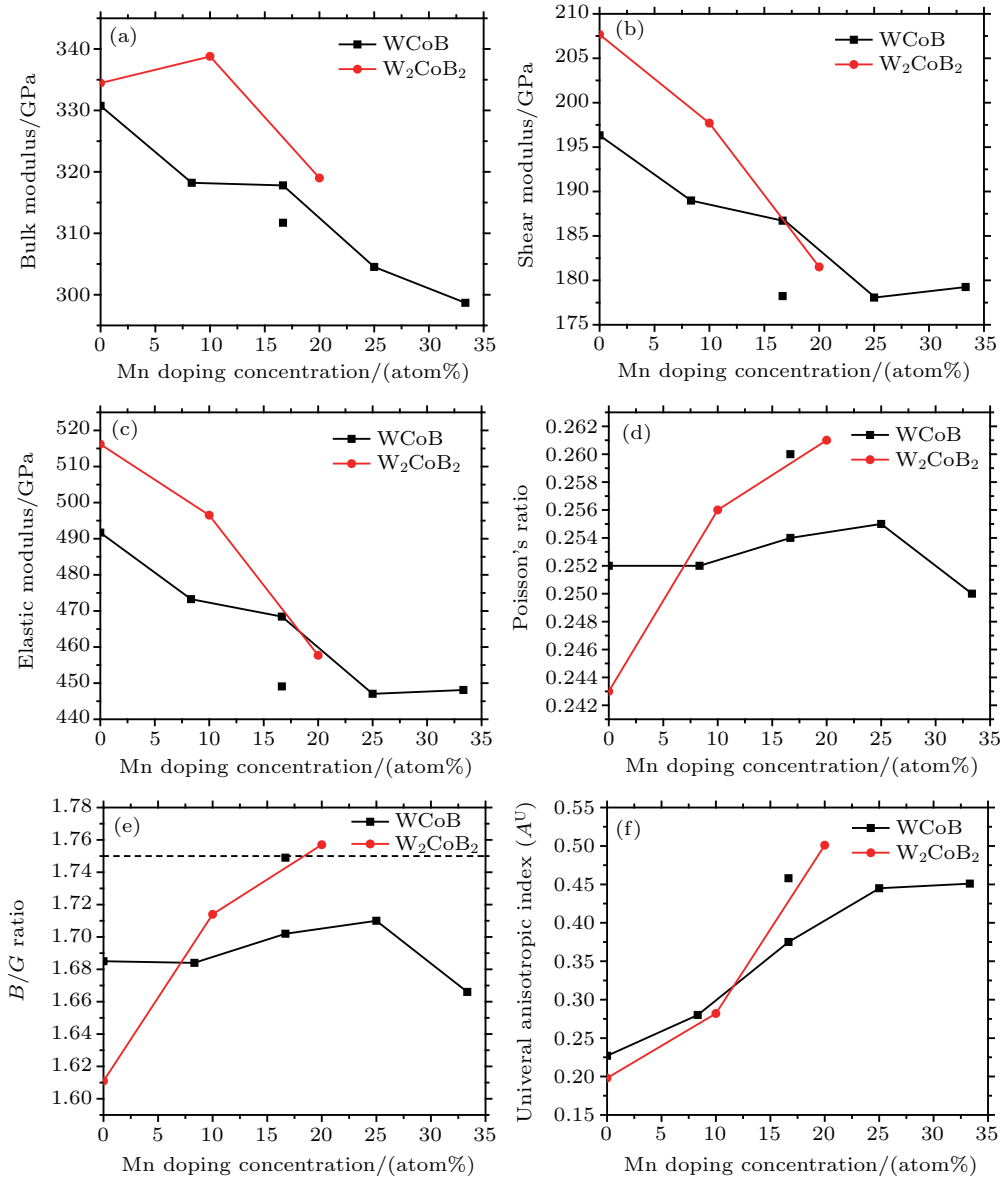


Fig. 2. (color online) Calculated values of (a) bulk modulus B (GPa), (b) shear modulus G, (c) Young's modulus E, (d) Poisson's ratio γ, (e) B/G ratio, and (f) universal anisotropic index (A^U) of $W_4Co_{4-x}Cr_xB_4$ and $W_4Co_{2-x}Cr_xB_4$.

The bulk modulus B and shear modulus G are calculated by Voigt–Reuss–Hill[36] approximation, which can be expressed by the following equations:

$$B = (B_V + B_R)/2, \tag{8}$$

$$G = (G_V + G_R)/2. \tag{9}$$

Young's modulus E and Poisson's ratio υ can be calculated from the following equations:

$$E = (9BG)/(3B+G), \tag{10}$$

$$\upsilon = (3B - 2G)/[2(3B+G)]. \tag{11}$$

A universal elastic anisotropy index (A^U) is proposed, which accounts for both the shear and bulk contributions, and is given below.

$$A^U = 5G_V/G_R + B_V/B_R - 6 \geq 0. \tag{12}$$

Table 3. Calculated elastic constants (in unit GPa) of $W_4Co_{2-x}Cr_xB_4$.

	g-$W_4Co_2B_4$	h-W_4CoMnB_4	i-$W_4Mn_2B_4$
C_{11}	588.06	618.78	563.35
C_{22}	601.75	585.91	587.05
C_{33}	538.17	497.05	452.6
C_{44}	239.93	248.97	254.87
C_{55}	247.14	239.53	236.48
C_{66}	209.22	184.82	136.96
C_{12}	157.69	179.68	167.94
C_{13}	248.73	258.77	250.68
C_{23}	235.1	237.1	217.67

The mechanical properties of Mn doping $W_4Co_{4-x}Mn_xB_4$ and $W_4Co_{2-x}Mn_xB_4$ are calculated and the results are shown in Tables 2 and 3, including bulk modulus, shear modulus, Young's modulus, and Poisson's ratio. The mechanical properties of the compounds are usually characterized by the full set of elastic constants. Three principle axes have relatively high elastic constants, indicating the high resistance to linear compression in these directions. However, the magnitude orders in three axes are different. For orthorhombic WCoB, the order is $C_{33} > C_{11} > C_{22}$, which shows the higher deformation resistance along the c axis than the a axis. With the increasing of Mn doping content, the elastic constant decreases slightly, indicating Mn doping reduces the deformation resistance along a, b, and c axes. The C_{12} increases clearly while C_{13} and C_{23} decrease distinctly with the increasing of the Mn doping content. In the case of orthorhombic W_2CoB_2, C_{22} is larger than C_{11} and C_{33}, suggesting the extremely large stiffness along the b axis. C_{11} increases when the Mn doping content is 10 at.%, indicating that the Mn doping leads to the higher deformation resistance along the a axis. A similar trend is also found separately in C_{12}, C_{13}, and C_{23}, implying that the Mn doping may have a positive effect on W_2CoB_2.

The calculated values of bulk modulus B, shear modulus G, Young's modulus E, Poisson's ratio γ, B/G, and universal anisotropic index (A^U) of WCoB and W_2CoB_2 are shown in Fig. 2. The isolate point refers to the crystal structure $W_4Co_2Mn_2B_4$-unsymmetry, which is more unstable than $W_4Co_2Mn_2B_4$-symmetry with higher cohesive energy. With the increasing of Mn doping content, Young's modulus, bulk modulus, and shear modulus of WCoB decrease slowly, which means that the Mn doping leads to lattice distortion and stress concentration, and thus reducing the resistance of deformation. Similarly, the bulk modulus and shear modulus of W_2CoB_2 decrease rapidly while Young's modulus increases at first, which means that the unstable structure contributes to the reduction of the mechanical properties.

Poisson's ratio can be used to analyze the brittleness of crystals.[37,38] For WCoB orthorhombic structure, it is clear that Poisson's ratio fluctuates around 0.25. However, with the increasing of Mn doping content, the Poisson ratio of W_2CoB_2 increases rapidly. Paugh[39] proposed that the ratio of B/G can be used to estimate the ductility and brittleness of material, and the criterion is about 1.75. Meanwhile, comparing the Poisson ratio with 0.25, the ductility of material can also be evaluated. We find that Mn doping increases the ductility of WCoB and W_2CoB_2, but all compounds are brittle except W_2MnB_2. Because ductile compounds usually have a high Poisson's ratio and high B/G ratio, Mn doping improves the ductility of W_2CoB_2, but shows little effect on the ductility of WCoB. The universal elastic anisotropy index (A^U) is identically zero for locally isotropic single crystals and the departure of A^U from 0 determines the extent of single crystal elastic anisotropy. The larger the value of A^U, the stronger the anisotropy of the compounds will be. Therefore, it is clear that higher Mn doping content leads to the increasing of anisotropy.

3.3. Population analysis and hardness

The population analysis can be used to evaluate the bonding strength among atoms, which can provide sufficient information about the chemistry bonding.[40] The overlap population of a covalent bond is bigger than an ionic bond, and both of them are larger than 0. When the overlap population is less than 0, it shows the existence of anti-bonding. Zhou[41] provided a method to analyze the chemical bonds among atoms by calculating the average overlap population n_{AB}, and the equation is as follows:

$$n_{AB} = \frac{\sum_i n_i^{AB} N_i}{\sum_i N_i}, \tag{13}$$

where N_i is the total number of A–B bonds and n_i^{AB} refers to the bond population of the A–B bond in the i type.

The calculated overlap population of bonds is listed in Tables 4 and 5. It is obvious that B–B bonds do not exist in Mn doping WCoB structure, which is caused by the long distance between atoms. With the increase of Mn doping content, the overlap population increases for most of the bonds, implying that the Mn atoms contribute to the increase of covalent properties for most of the bonds. The negative population means that a strong repulsion force exists among these bonds and it also increases with the increase of Mn doping content. It is clear that the average overlap population decreases when Mn atoms replace Co atoms and form bonds, so Mn doping reduces the covalency of crystal. Similarly, we find that the same trend occurs in the Mn doping W_2CoB_2 compounds, indicating that WCoB and W_2CoB_2 have similar properties.

Table 4. Calculated overlap population of bonds for $W_4Co_{4-x}Mn_xB_4$.

	a-$W_4Co_4B_4$	b-$W_4Co_3MnB_4$	c-$W_4Co_2Mn_2B_4$	d-$W_4Co_2Mn_2B_4$	e-$W_4CoMn_3B_4$	f-$W_4Mn_4B_4$
B–B	–	–	–	–	–	–
B–Co	0.307	0.316	0.307	0.337	0.33	–
B–W	0.533	0.561	0.582	0.593	0.612	0.64
B–Mn	–	0.117	0.16	0.11	0.146	0.16
Co–Co	–0.150	–0.14	–0.14	–	–	–
Co–W	–0.0525	–0.0275	–0.045	0.0175	0.015	–
Co–Mn	–	–0.3	–	–0.27	-0.25	–
W–W	–0.160	–0.105	–0.11	-0.03	0.025	0.07
W–Mn	–	–0.15	–0.095	-0.1575	–0.103	–0.0725
Mn–Mn	–	–0.185	–0.175	–	–0.36	–0.33

Table 5. Calculated overlap population of bonds for $W_4Co_{2-x}Mn_xB_4$.

	g-$W_4Co_2B_4$	h-W_4CoMnB_4	i-$W_4Mn_2B_4$
B–B	0.56	0.55	0.53
B–Co	0.42	0.47	–
B–W	0.265	0.28	0.295
B–Mn	–	0.23	0.29
Co–Co	–	–	–
Co–W	0.03	0.025	–
Co–Mn	–	–	–
W–W	-0.11	-0.045	0.015
W–Mn	–	-0.105	-0.085
Mn–Mn	–	–	–

Hardness of Mo_2FeB_2 ternary boride hard alloy is dominated by Mo_2FeB_2 hard phase, which comes from the Mn doping Mo_2FeB_2 structure, and has been proved by Lin's[24] research. As is well known, the hardness is a macroscopic property, so different hardness models including some models established on population, are used for evaluation and comparison. In 1954, Pugh[42] established a hardness model by using the shear modulus, which can be expressed by $H_v = 0.151\,G$. Chen[43] modeled the hardness by introducing Pugh's ratio, $k = G/B$, which can be used to evaluate the brittleness/ductility of a material, and established a hardness model, which can be expressed as follows:

$$H_v = 2(k^2G)^{0.585} - 3, \tag{14}$$

where k is Pugh's ratio and G is the shear modulus.

However, Gao[44] established another hardness model, with the resistance assumed to be proportional to the homopolar energy gap. Gao also suggested that the strength of a bond can be characterized by using average overlap populations, where the overlap population is evaluated by the first principles. The following expressions are used to evaluate the hardness of materials:

$$H_\gamma^\mu\,(\mathrm{GPa}) = AP^\mu\left(\gamma_b^\mu\right)^{-5/3}, \quad A = 740, \tag{15}$$

$$\gamma_b^\mu = (d^\mu)^3 / \sum_\mu (d^\mu)^3 N_b^\mu, \quad N_b^\mu = N^\mu/\Omega, \tag{16}$$

where: H_γ^μ is the hardness of the μ type bond; d^μ is the bond length of the μ type bond; N_b^μ is the bond density per cubic angstroms of the μ type bond; Ω is the cell volume; and P^μ is the overlap population of the μ type bond. Moreover, because the hardness of a metallic bond is ill-determined in the first-principles calculation, the hardness of metallic bonds is not considered in some situations. The hardness of material can be expressed as the geometric average of all bond hardness, where m_n is the bond number of μ type bond.

$$H_\gamma^\mu\,(\mathrm{GPa}) = \left[(H_\gamma^{\mu_1})^{m_1}(H_\gamma^{\mu_2})^{m_2}\ldots(H_\gamma^{\mu_n})^{m_n}\right]^{1/(m_1+m_2+m_3)}. \tag{17}$$

So we use three hardness models to evaluate the hardness of material and explore the effects of Mn doping content on overlap population and hardness of WCoB and W_2CoB_2. The isolate point refers to the crystal structure $W_4Co_2Mn_2B_4$-unsymmetry, which is more unstable than the $W_4Co_2Mn_2B_4$-symmetry with higher cohesive energy.

By using three different hardness models, the hardness of materials is characterized to explore the influence of different Mn doping content. The hardness models are established for binary oxide and they might not be suitable for ternary boride. So the results are compared to find the hardness change of WCoB and W_2CoB_2 ternary boride.

For WCoB ternary boride, Paugh's and Chen's models are based on the bulk modulus and shear modulus, which has

been discussed above. It is obvious that the hardness decreases with the increasing of Mn doping content, due to the decreasing of bulk modulus and shear modulus. Gao's model shows a similar trend of hardness, and the decreasing range is even larger. For W_2CoB_2 ternary boride, Paugh's and Chen's models show the hardness decreasing rapidly, which is similar to the trend of bulk modulus and shear modulus. However, Gao's model shows that the change of hardness is minor, so it can be concluded that Mn doping does not improve the hardness of W_2CoB_2.

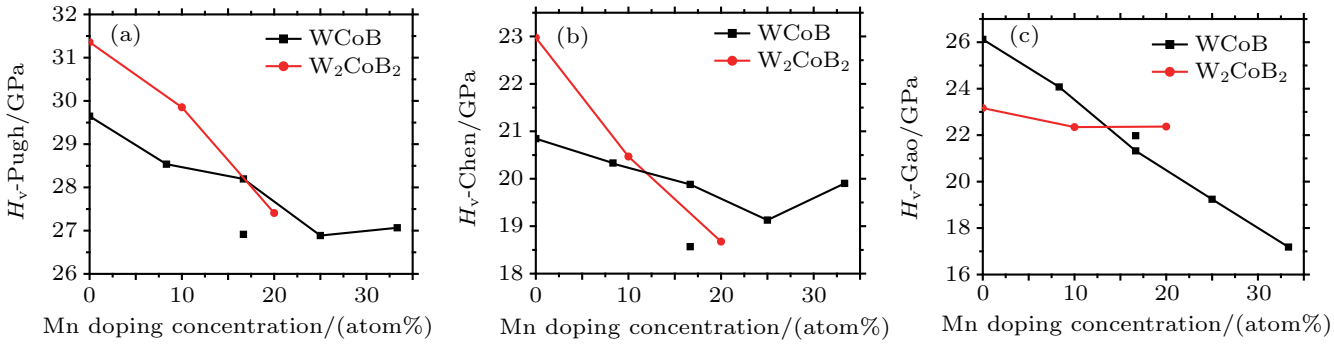


Fig. 3. (color online) Plots of theoretical hardness versus Mn doping concentration of WCoB and W_2CoB_2, obtained by different models: (a) H_v-Pugh, (b) H_v-Chen, (c) H_v-Gao.

In the analysis of average overlap population, we find that the higher Mn doping content leads to the higher population. However, when we study the effect of Mn doping content on WCoB and W_2CoB_2, the hardness decreases obviously, which can be verified by three different models. It is likely to be triggered by the increasing of bond length, which is caused by the larger atom radius of Mn ($r = 161$ pm) than Co ($r = 152$ pm) and weaker B–Mn covalent bond and W–Mn metallic bond, which is discussed in the next part.

After all, the hardness may be one of the most important properties which can be characterized by the first-principles calculation, and is hardly improved with craft. Compared with the study of Cr doping WCoB ternary boride[45] by first principles, the B/G ratio increases rapidly and reaches a value beyond 1.75, and the hardness decreases slightly. So the decreasing of hardness implies that Mn doping is not a suitable way to improve mechanical properties of WCoB ternary boride, which is also proved by the electronic structure and population analysis. If Mn doping cannot cause the solid solution to significantly strengthen nor grain refinement to form in WCoB hard alloy, Mn may not be a suitable choice for transition metal doping.

3.4. Density of states

The electronic propreties of WCoB and W_2CoB_2 with different Mn doping content are presented by calculating the density of states (DOS) and partial density of states (PDOS), which can help to reveal the effect of Mn doping content as shown in Figs. 4 and 5. The location of the dashed line represents the Ferimi level (E_F), and the deep valley at the Fermi level is known as the pseudogap (E_p). The electrons occupying the orbits above the pseudogap become delocalized, and the compounds will be metallized. The larger dispalcement of pseudogap between the Fermi level contributes to a higher hardness and covalence, which is usually composed of d–d electrons. Yu[46] studied the relationship between the value of density of states at the Fermi level and the stability of materials, and the result shows that the lower value is realted to the higher stability of noncrystal and quasi-crystal. However, WCoB and W_2CoB_2 compounds are typical crystals, so their value of the density of states at the Fermi level cannot be used to judge the stability of WCoB nor W_2CoB_2 with different Mn doping content.

The density of states (DOS) and partial density of states (PDOS) can be made more visual to be analyzed by dividing the density of states into different peaks. So it is clear that there are 9 distinct state peaks located near −8.5 eV, −6 eV, −4 eV, −3 eV, −2.3 eV, −0.8 eV, 1 eV, 2.3 eV, and 5.3 eV (named P_1, P_2, P_3, P_4, P_5, P_6, P_7, P_8, and P_9, respectively). The DOS at the Fermi level is not equal to 0, which shows the metallic character for each of the calculated Mn doping WCoB structures. Compared with the undoped WCoB structure in Fig. 4, it is obvious that these peaks can be divided into two groups.

The density of states at each of P_1, P_2, P_3, P_8, and P_9 vary slightly with the increasing of Mn doping content. The composition of P_1 is mainly composed of B-2s and W-5d orbitals and the compositions of P_2 and P_9 are made up of B-2p and W-5d orbits. There exists a strong hybridization at each of P_1, P_2, and P_9 between B and W, and these B–W covalent bonds between metal and non-metal are beneficial to shear modulus and hardness. The P_3 and P_8 are mainly composed of B-2p and W-5d orbits, and are affected by Mn-3d and Co-3d orbits. The W–Mn and W–Co metallic bonds have negative effects on shear modulus and hardness.

The P_4 is composed of W-5d, Co-3, and Mn-3d orbits

and a small amount of B-2p, and represents the metallization at −3 eV. The P_4, P_5, and P_6 are composed of W-5d, Co-3d, and Mn-3d orbits. The P_6 is mainly comprised of Co-3d orbits and decreases distinctly with the increase of Mn doping content and the decrease of Co content. However, the variations of P_4 and P_5 are minor, because the increase of Mn-3d counteracts the decrease of Co-3d. According to Fig. 4, P_4, P_5, P_6, P_7 and P_8 possess metal-to-metal bonding between W, Co, and Mn, which gives a negative contribution to the shear modulus. However, the effect of Mn doping is counteracted by the decrease of Co content, so the effect of Mn doping is extremely small except P6, which is affected by the decrease of the Co content. These results are consistent with the mechanical properties and overlap population analysis.

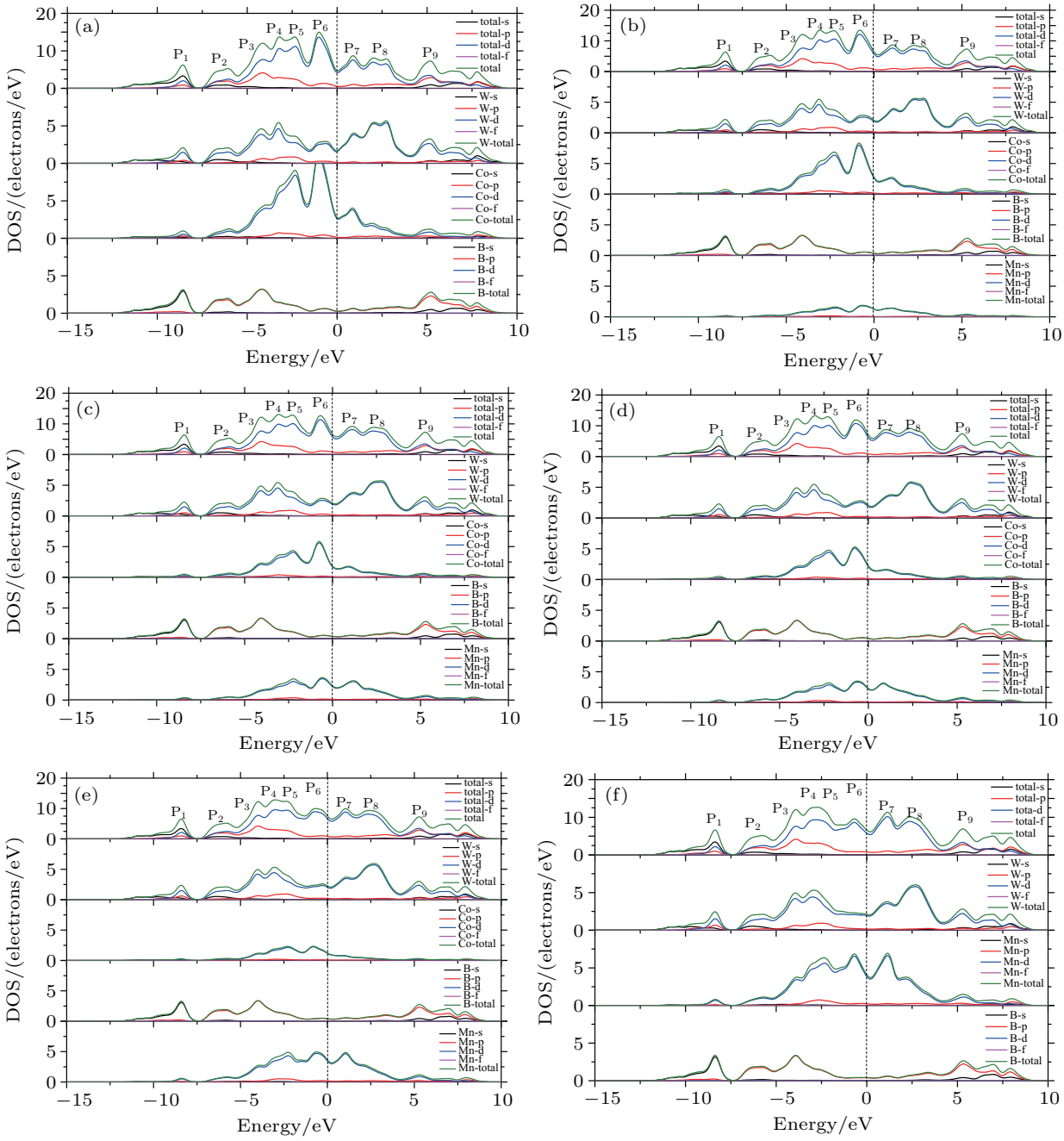


Fig. 4. (color online) Plots of total and partial density of states of WCoB with different Mn doping contents (a-$W_4Co_4B_4$, b-$W_4Co_3MnB_4$, c-$W_4Co_2Mn_2B_4$, d-$W_4Co_2Mn_2B_4$, e-$W_4CoMn_3B_4$, and f-$W_4Mn_4B_4$).

As shown in Fig. 5, it is found that the trends of DOS and PDOS for Mn doping W_2CoB_2 are similar to those in Mn doping WCoB. There are 7 distinct state peaks located near −10.4 eV, −3.8 eV, −2.4 eV, −0.56 eV, 2.2 eV, 4.3 eV, and 7.6 eV. It is clear that P1 is a relatively obvious resonance peak forming between B-2s and B-2p orbitals, forming the B-B covalent bond and contributing to the hardness for the Mn doping WCoB structure, which is consistent with the overlap population analysis. The P_2, P_6, and P_7 are composed of the strong hybridized B-2p, W-5d, Co-3d, and Mn-3d orbits, forming the

strong covalent bonds, giving a positive contribution to the shear modulus. Because the effect of Mn doping is counteracted by the Co content, the hybridization intensity does not weaken with the variation of Mn content. The P_3, P_4, and P_5 are made up of the W-5d, Co-3d, and Mn-3d orbits, and form metallic bonds between W, Co, and Mn, which makes a negative contribution to the shear modulus. Due to the decrease of Co content, P_4 decreases with the increasing of Mn doping content, which is consistent with the analysis of B/G and Poisson' ratio.

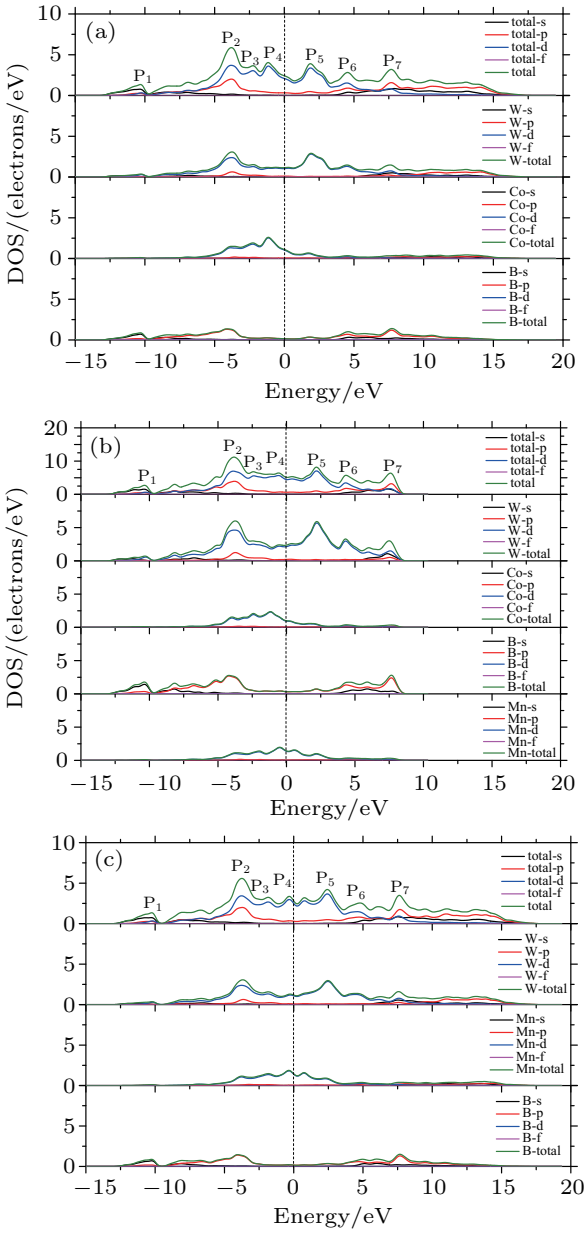


Fig. 5. (color online) Plots of total and partial density of states versus energy of W_2CoB_2 with different Mn doping contents g-$W_4Co_2B_4$, h-W_4CoMnB_4, i-$W_4Mn_2B_4$ shown in panels (a)–(c).

3.5. Charge density difference

The charge density difference between Mn doping WCoB and W_2CoB_2 is calculated and discussed to explore the bond characteristics, which are shown in Figs. 6 and 7. Figure 6 shows the charge density difference of Mn doping WCoB along the (1 0 0) plane[47] at different doping contents, and the crucial atoms and bonds are labeled. Because crystal structures have a periodic arrangement, the characteristic can be shown by different cross-sections. The red color represents the maximum delocalization of electrons, and the blue color refers to the maximum localization of electrons. The white color means that the electron density is almost zero.[48]

The B–Co bonds and W–Co bonds are typical bonds in Fig. 6, and the bond length of B–Co bonds and W–Co bonds are up to 2.689 Å and 2.201 Å, respectively. With the increase of Mn doping content, the bond lengths of B-Co and W–Co increase slightly, which contributes to the decrease of hardness. Moreover, the number of BMn bonds and W–Mn bonds increase with the increase of Mn content, resulting in the increase of the bond length and crystal volume. However, when the alloying content reaches a maximum value of 33% at.%, Mn atoms will replace Co atoms completely, and thus forming the stronger B–Mn and W–Mn bonds, which indicates the increase of Young's modulus and shear modulus after their sharp decrease.

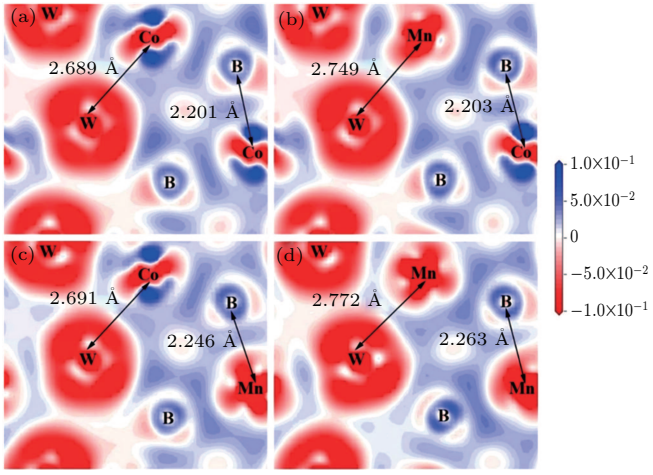


Fig. 6. (color online) Illustration of charge density difference of Mn doping WCoB at different structure: (a) $W_4Co_4B_4$-a, (b) $W_4Co_3MnB_4$-b, (c) $W_4Co_2Mn_2B_4$-c, and (d) $W_4CoMn_3B_4$-e.

The charge density differences among different structures of Mn doping W_2CoB_2 are shown in Fig. 7. The atoms in italics show that they are not on the cross-section, and their position is the projection on the cross-section. It is clear that B–Co bonds and W–Co bonds are typical bonds in W_2CoB_2, and their bond lengths are up to 2.090 Å and 2.693 Å, respectively. With the increase of Mn doping content, Mn will replace Co atoms gradually. The bond lengths of B–Mn bonds and W–Mn bonds are slightly larger than B–Co bonds and W-Co bonds, respectively. When the Mn doping content is up to 20 at.%, all Co atoms have been replaced by Mn atoms completely, indicating the increase of the number of W–Mn metallic bonds, which is harmful to mechanical properties. This result is consistent with the previous analysis of density of states and partial density of states.

The calculated electronic structure implies that the Mn doping atoms mainly form B–Mn bonds and W–Mn bonds with the adjacent B atoms and W atoms respectively. Because the average overlap population analysis indicates that Mn doping reduces the covalency of crystal, the formation of B–Mn covalent bonds and W–Mn metallic bonds make negative contributions to mechanical properties. When the Mn doping content reaches a maximum value, the formation of the stronger B–Mn bonds and W–Mn bonds may improve the mechanical properties slightly after their sharp decreasing.

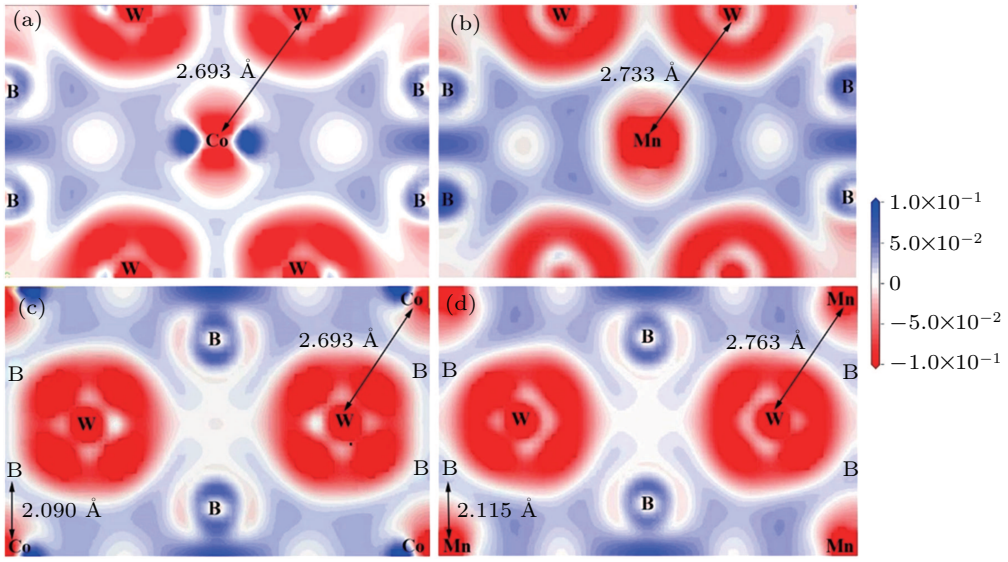


Fig. 7. (color online) (color online) Illustration of charge density difference of Mn doping W_2CoB_2 at different structure: (a) $W_4Co_2B_4$-g, (b) W_4CoMnB_4-h, (c) $W_4Co_2B_4$-g, and (d) $W_4Mn_2B_4$-i.

4. Conclusions

In this work, the first-principles calculation is employed to investigate the influence of the Mn doping content on the mechanical properties and electronic structure of WCoB and W_2CoB_2. Some conclusions are drawn as follows.

(i) By calculating cohesive energy and formation energy, it is found that all the structures can retain structural stability at different Mn doping content. With the increase of Mn doping content, the stability of the crystal structure increases slightly. However, the increasing trend of formation energy indicates that the Mn doping structures are harder to generate in the formation progress.

(ii) According to the analysis of calculated mechanical properties, almost all mechanical properties decrease with the increase of Mn doping content, which is mainly ascribed to the weak B–Mn covalent bonds. The increase of Mn doping content improves B/G and Poisson's ratio slightly, which can be attributed to the weak W–Mn metallic bonds. Three different hardness models show that the increase of Mn doping content reduces the hardness of WCoB and W_2CoB_2.

(iii) The population analysis shows that the Mn doping leads to the increase of bond population. However, the formation of weaker B–Mn covalent bonds and W–Mn metallic bonds result in the decrease of mechanical properties, which is also proved by DOS, PDOS, and charge density difference. When the Mn doping content reaches a maximum value, all Co atoms can be replaced by Mn atoms and the structures turn into WMnB and W_2MnB_2, respectively, which leads to the slight increase of mechanical properties.

References

[1] Takagi K 2006 *J. Solid State Chem.* **179** 2809
[2] Yamasaki Y, Nishi M and Takagi K 2004 *J. Solid State Chem.* **177** 551
[3] Nishiyama K, Keino M, Furuyama Y, et al. 2003 *J. Alloys Compd.* **355** 97
[4] Takagi K, Ohira S, Ide T, Watanabe S and Kondo Y 1987 *Metal Powder Rep.* **42** 483
[5] Komai M, Yamasaki Y, Takagi K I and Watanabe T 1992 *Adv. Powder Metal. Particulate Mater.* **8** 81
[6] Tashiro H, Hirata K, Yamasaki Y and Takagi K 2007 *Mater. Sci. Forum. Trans. Tech. Pub.* **534** 377
[7] Haschke H, Nowotny H and Benesovsky F 1966 *Monatshefte für Chemie und verwandte Teile anderer Wissenschaften* **97** 1459
[8] Hofmann H and Petzow G 1986 *J. Less Common. Metals* **117** 121
[9] Zahariev Z T and Marinov M I 1993 *J. Alloys Compd.* **201** 1
[10] Hu B, Pan Y, Wang Q, Zhou H and Xu M 2011 *Heat Treat. Metals* **6** 008
[11] Takagi K 1987 *Int. J. Powder Met.* **23** 157
[12] Ke D Q, Pan Y J, Xu Y Y, Yang L and Wu R 2017 *Appl. Mech. Mater. Trans. Tech. Pub.* **872** 56
[13] Yu H, Zheng Y, Liu W, Zheng J and Xiong W 2010 *Mater. Design* **31** 2680
[14] Yu H, Zheng Y, Liu W, Zheng J and Xiong W 2010 *Int. J. Refrac. Metals Hard Mater.* **28** 286
[15] Yamasaki Y, Nishi M and Takagi K 2004 *J. Solid State Chem.* **177** 551
[16] Yang F, Wu Y, Han J and Meng J 2016 *J. Alloys Compd.* **665** 373
[17] Takagi K 2003 *Metals Mater. Int.* **9** 467
[18] Komai M, Isobe Y and Takagi K 1993 *J. Jpn. Soc. Powder Powder Metallurgy* **40** 38
[19] Ke D, Pan Y, Lu X, Hong B and Zhang H 2015 *Cera. Int.* **41** 15235
[20] Wang X, Chen C, Feng S, Wei X and Li Y 2017 *Chin. Phys. B* **26** 127402
[21] Zhang Z X, Zhang Y, Xue W H, Jia W, Zhang C L, Li C X and Cui P 2017 *Chin. Phys. B* **26** 123102
[22] He W, Huang H, Liu Z and Ma X 2018 *Chin. Phys. B* **27** 016201
[23] Xuan S K 2017 *Acta Phys. Sin.* **66** 237401 (in Chinese)

[24] Lin Y H, Tong C C, Pan Y, Liu W Y and Singh A 2017 *Mod. Phys. Lett. B* **31** 1750138
[25] Wang S, Pan Y, Lin Y and Tong C 2018 *Comput. Mater. Sci.* **146** 18
[26] Xu Y, Pan Y, Ke D, Yang L and Wang P 2017 *Mater. Sci. Technol.* **25** 59
[27] Hohenberg P and Kohn W 1965 *Phys. Rev.* **136** B864
[28] Kohn W and Sham L J 1965 *Phys. Rev.* **140** A1133
[29] Perdew J P, Burke K and Ernzerhof M 1996 *Phys. Rev. Lett.* **77** 3865
[30] Vanderbilt D 1990 *Phys. Rev. B* **41** 7892
[31] Kuzma I B and Chepiga M V 1969 *X-ray investigation of the tungsten-iron-boron and tungsten-cobalt-boron systems*. Lvov State Univ., 1969
[32] Rieger W, Nowotny H and Benesovsky F 1966 *Monatshefte für Chemie und verwandte Teile anderer Wissenschaften* **97** 378
[33] Monkhorst H J and Pack J D 1976 *Phys. Rev. B* **13** 5188
[34] Wu Z, Zhao E, Xiang H, Hao X, Liu X and Meng J 2007 *Phys. Rev. B* **76** 054115
[35] Ravindran P, Fast L, Korzhavyi P A and Johansson B 1998 *J. Appl. Phys.* **84** 4891
[36] Hill R 1952 *Proc. Phys. Soc. A* **65** 349
[37] Lewandowski J J, Wang W H and Greer A L 2005 *Phil. Mag. Lett.* **85** 77
[38] Wang J X, Chen Z B and Gao Y C 2018 *J. Phys. Chem. Solids* **116** 72
[39] Aouadi S M 2006 *J. Appl. Phys.* **99** 053507
[40] Reuss A 1929 *J. Appl. Math. Mech.* **9** 49
[41] Zhou C T, Xing J D, Xiao B, Feng J, Xie X J and Chen Y H 2009 *Comput. Mater. Sci.* **44** 1056
[42] Pugh S F 1954 *London, Edinburgh Dublin Phil. Mag. J. Sci.* **45** 823
[43] Chen X Q, Niu H, Li D and Li Y 2011 *Intermetallics* **19** 1275
[44] Gao F, He J, Wu E, Liu S, Yu D, Li D, Zhang S and Tian Y 2003 *Phys. Rev. Lett.* **91** 015502
[45] Zhang T, Yin H, Zhang C, Qu X H and Zheng Q J 2018 *Mod. Phys. Lett. B* **2018** 1850240
[46] Yu H B, Wang W H and Bai H Y 2010 *Appl. Phys. Lett.* **96** 081902
[47] Jiang P G, Wang Z B, Yan Y B and Liu W J 2017 *Acta Phys. Sin.* **66** 246801 (in Chinese)
[48] Xu W W, Han J J, Wang Y, Wang C P, Liu X J and Liu Z K 2013 *Acta Materialia* **61** 5437